Dehydration-Driven Morphological Transformation of Flexible Vesicles on Liquid−Solid Interface

Jiaye Su,*[,†] Jingyuan Chen,[‡] and Zhenwei Yao*[,‡]

[†]Department of Applied Physics, Nanjing University of Science and Technology, Nanjing, Jiangsu 210094, China
[‡]School of Physics and Astronomy, Institute of Natural Sciences, Shanghai Jiao Tong University, Shanghai 200240, China

ABSTRACT: Understanding deformation mechanisms of flexible vesicles has strong connections with a host of problems in materials geometry and biology. A setting of particular interest is an adsorbed vesicle on a liquid−solid interface. The dehydration process, which is a common phenomenon for a vesicle immersed in salt solution, will reshape the vesicle. In this work, using the combination of large-scale explicit-solvent coarse-grained molecular dynamics simulations and analytical theory, we systematically investigate the controllable morphological transformation of both fluid and crystalline vesicles adsorbed on the liquid−solid interface under slow and fast dehydration rates. We observe the bifurcation in the deformation of these two types of vesicles under slow and fast dehydration modes. Specifically, we find inward-buckling-driven large deformations, including stomatocyte-like shapes for fluid vesicles and double-layered bowl-like and conelike shapes for crystalline vesicles. We have also analyzed the analytically tractable spreading process of a fluid vesicle on the interface, and our theoretical results agree well with numerical observations. This work demonstrates the promising possibility of using the combination of surface adsorption and the dynamic dehydration protocol to enlarge the vesicle shape space. It has implications toward versatile control and engineering of vesicles on the interface.
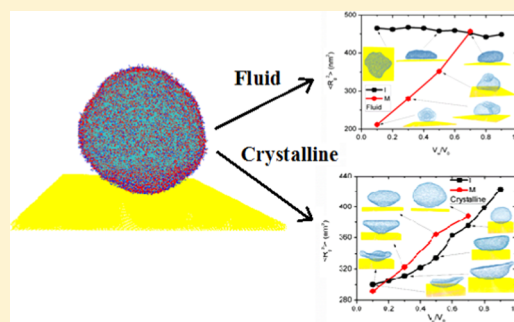
INTRODUCTION

Flexible vesicles via self-assembly of various amphiphilic molecules in the aqueous environment can develop a myriad of morphologies that are highly adaptive to lipid types,[1,2] lipid−water interactions,[3] pH values of solutions,[4] salt concentrations,[5] and ambient pressures and temperatures.[6] The rich morphologies of vesicles create a multitude of possibilities for functionalization in diverse fields ranging from encapsulation[7−9] and drug delivery[10,11] to the realization of relevant biological processes such as endocytosis.[12,13] Over the past decades, the confluence of experimental, theoretical, and computational efforts in synthesis, characterization,[14−21] and modeling[22−25] of both liquid and crystalline vesicles has greatly enriched our understanding of the governing principles of vesicle organization. Notably, advanced modern computational technology like coarse-grained molecular dynamics (CGMD) simulations[1,3,26−28] and dissipative particle dynamics simulations[29] allows us to investigate small-scale vesicles down to the molecular level and to explore the regime inaccessible by the current experimental technique.[25] While the shape space of free-standing vesicles in bulk solution has been extensively studied experimentally and theoretically, understanding morphological transformation of a flexible vesicle on a liquid−solid interface represents an important research direction that has strong connections with a host of problems in materials geometry and biology.[30−37] Notably, vesicle adsorption on various substrates provides an important

approach to fabricate supported lipid bilayers, which has extensive applications.[38]

The goal of this work is to investigate the adaptive morphology of a draining flexible vesicle on the liquid−solid interface. Permeation of water is inevitable for a vesicle immersed in salt solution.[39−41] We focus on the combined effects of the draining process and interface affinity on the vesicle morphology. We employ computer simulations based on the explicit-solvent CGMD in combination with analytical elasticity theory. Specifically, we design a model system composed of ionic amphiphiles [−1 palmitic acid (C_{15}−COOH) and +3 trilysine (C_{16}−K_3)] and water molecules. The draining process is modeled by controllable dynamic dehydration protocols at varying rates. Here, we note that, in its reshaping for the optimal morphology in the dehydration process, the vesicle changes its volume but maintains a fixed surface area, which is opposite for an ordinary liquid droplet.

The main results about the morphology of such a special droplet realized in both systems of fluid and crystalline vesicles are presented below. We numerically observe the bifurcation in the deformation of both types of vesicles under the slow and fast dehydration modes. Specifically, a fluid vesicle evolves into stomatocyte-like shapes under massive removal of water and continuously spreads on the substrate in a slow dehydration

rate. The latter process is analytically analyzed using elasticity theory, and the theoretical results agree well with numerical observations. For a crystalline vesicle, we find that the interplay of the rigidity of crystalline order and the interface affinity leads to morphologies distinct from that of a fluid vesicle. Notably, our simulations capture the inward buckling process of an initially spherical crystalline vesicle toward double-layered bowl-like and conelike shapes sitting on the interface. We have also discussed the energetics in the deformation of the vesicles. These results demonstrate the promising possibility of using the combination of surface adsorption and the dynamic dehydration protocol to enlarge the vesicle shape space. This study has implications toward versatile control and engineering of vesicles on the interface.

MODEL AND SIMULATION METHOD

Figure 1 shows our simulation system, where an ionic vesicle filled with water is adsorbed on a hydrophilic surface (SiO_2),
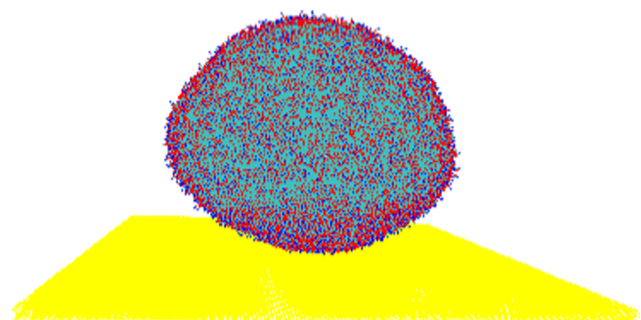
Figure 1. Plot of a typical initial configuration of the vesicle adsorbed on the SiO_2 surface in a water box ($70 \times 70 \times 52$ nm^3) using periodic boundary conditions. Water is not shown for clarity. The size of the vesicle is about 47 nm (outer diameter).

and the water molecules are not shown for clarity. The present bilayer vesicles are composed of ionic amphiphiles, i.e., −1 palmitic acid (C_{15}−COOH) and +3 trilysine (C_{16}−K_3), same as our previous work,[25] where the shape transformations in bulk solution are systematically investigated through a controllable dynamic protocol to change the inner water volume. Both of the fluid and crystalline vesicles exhibit rich morphologies by dynamically changing the volume. The vesicles are electroneutral systems with 30% average ionization of the palmitic acid molecules, corresponding roughly to pH value 4 of the experimental system,[33] where the melting temperature is about 328 K. We thus run the simulations for fluid vesicles at 350 K and for crystalline vesicles at 300 K. We consider a large vesicle with an outer radius of 23.5 nm (containing 3000 +3 lipids, 9000 −1 lipids, and 21 000 neutral lipids) for most of the simulations, a 14 nm (with 1/3 lipid number) and a 9 nm (1/6 lipid number) radius for selected runs, yielding systems of 6.1×10^4 to 2.1×10^6 particles.

The bilayer membranes are semipermeable, and water can even permeate through them by thermal fluctuations.[39] Under a given driving force, e.g., osmotic difference between the inner compartment and outside medium, water will diffuse across the membrane, exemplified by our recent simulation work,[40] leading to the change of vesicle's volume-to-surface ratio and subsequent shape change as shown in experiments.[5,42] Similar to our previous work,[25] to speed up the osmotic process, we remove some water inside the vesicle and perform CGMD

runs to obtain stable shapes. Specifically, the inner water volume is changed by two distinct dynamic protocols, i.e., incrementally (I) and massively (M), which can be analogous to low and high salt (or extra extracting energy involved) conditions in experiments, respectively. Actually, the I protocol indicates a step-by-step removal with 10% inner water in each step, and the final equilibrated vesicle shape is used as the initial state for the next step until the target remaining water amount. The M protocol means the direct removal of the given amount of water. Herein, for both fluid and crystalline vesicles, I and M protocols lead to thoroughly different vesicle shapes that are not seen in bulk solutions.[25]

Although it is difficult to define or determine the fast and slow dehydration rates, the I and M protocols can be corresponding to the slow and fast dehydration rates, respectively. Similar to our previous work,[25] we remove the water molecules uniformly from the whole inner water volume, where the bilayer membrane can be well relaxed with the motion of inner water and therefore can well reproduce experimental vesicle shapes. Our previous work demonstrated a quite different shape when removing the surface part of the inner water volume. This method can lead to a vacuum bubble near the bilayer wall and thus induce a sudden collapse or even rupture (for sufficiently large vesicle and bubble size) of the vesicle. There are also other methods to remove the inner water (e.g., remove some local parts simultaneously) to reach different metastable states of the vesicle and create richer morphologies.

All molecular dynamics (MD) simulations were performed by the Gromacs 4.6.7 software package[43] and the MARTINI coarse-grained force field (version 2.1).[44−46] The pressure (1 bar) and temperature were controlled by the Berendsen method.[47] The periodic boundary conditions were applied in all directions. The MARTINI force field is generally based on the four-to-one mapping rule, i.e., four heavy atoms are represented by one single interaction bead. Four interaction types (polar, intermediate polar, apolar, and charged) and some subtypes are classified according to the hydrogen-bonding capability or the degree of polarity. The mapping methodology of the present lipids can be found in the previous work.[33] The SiO_2 surface contains OH residues and thus we used P4 type to represent its hydrophilic nature; while other SiO_2 molecules were modeled by hydrophobic C1 type. For the protocol I, we conducted 150 ns MD runs for each step, and the final state was used as the initial state of the next step. For the protocol M, we performed 300 ns MD run for each system. We checked the vesicle shape and potential energy to ensure the stability after the change of water volume. All of the simulation data were averaged by two independent MD runs with different initial vesicle states. The standard error bars were mostly trivial and smaller than the data symbols. Therefore, the vesicle shape, size, and energy should be stable and mainly determined by the water volume inside the vesicle. We believe that the results should be a direct examination or proof to validate the simulation model and method. Our previous work showed excellent agreement between the simulation results and experiments for the fluid vesicle in bulk solution.[25] Specifically, the fast and slow dehydration rates lead to a series of distinct vesicle shapes that resemble experimental observations. Therefore, our CG model and simulation method should be reasonable.

■ RESULTS AND DISCUSSION

A flexible vesicle filled with water shrinks and deforms in the dehydration process. Such a volume-driven shape transformation has recently been reported for fluid vesicles immersed in bulk solution.[1,3,25,29] In combination with the affinity of the interface, a draining vesicle adsorbed on the liquid−solid interface is expected to develop even richer morphologies under the volume-driven mechanism. In our simulations, a typical initial configuration of the vesicle on the SiO$_2$ surface is shown in Figure 1. The obtained vesicles in our simulations are quite stable at least over the data collection time of 100 ns. These vesicles may represent metastable states sitting deep in the energy valleys. In this section, we first discuss the morphological transformation of fluid vesicles in the dehydration process from the perspectives of the mean-squared radius of gyration and the characteristic geometric parameters, followed by energetics analysis. We then present the results of the crystalline vesicle. Finally, we briefly discuss the influence of adsorption strength and vesicle size on the morphology of crystalline vesicles.

Shape Transformations of Fluid Vesicles. In Figure 2, we show the mean-squared radius of gyration $\langle R_g^2 \rangle$ of the
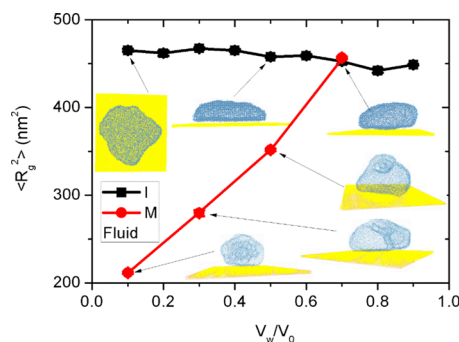
Figure 2. Plot of the mean-squared radius of gyration of a fluid vesicle on a SiO$_2$ substrate versus V_w/V_0. V_w is the volume of the vesicle, and V_0 is the initial volume of the vesicle before dehydration occurs. The symbols I and M indicate the two dynamic protocols to remove water from the vesicle in simulations.

vesicle as a function of the water volume ratio V_w/V_0 under the two designed dynamic protocols I and M, respectively. V_0 is the initial water volume before removal and V_w denotes the virtual water volume after removal. We actually counted the number of water molecules instead of water volume, which is more simple and doable. This is because the volume ratio V_w/V_0 is the same as the number ratio. For the protocol I, with the incremental decrease of the enclosed water and thus the vesicle volume, the vesicle gradually spreads on the interface under the strong lipid−surface interaction, resembling the behavior of a liquid drop on a solid substrate under gravity. In this process, the value of $\langle R_g^2 \rangle$ is almost invariant for the protocol I. In contrast, for a free-standing fluid vesicle in solution, dehydration leads to its elongation in the sequence of a sphere, an elliptocyte (or prolate), and a cigarlike or a dumbbell-like shape, and ultimately to a double-layer disk.[25] Note that the transition to the double-layer disk indicates the change of the volume-reduction mode; the one-dimensional elongation of the vesicle seems insufficient with the continuing dehydration. In the transition between the last two shapes, the $\langle R_g^2 \rangle$-curve is peaked.[25]

Figure 2 also shows a clear bifurcation in morphological transformation of the fluid vesicle when using different protocols. With the protocol M, the fluid vesicle evolves along a distinct sequence characterized by inward buckling instead of gradual shape transformation as in the protocol I. Specifically, when $V_w/V_0 < 0.7$, the vesicle starts to deform toward stomatocyte shapes resembling those found in free-standing vesicles in bulk solution.[25] However, at $V_w/V_0 = 0.5$, a small stomatocyte has developed locally on the top of the vesicle (see the inset of Figure 2). In contrast, the free-standing vesicle becomes a whistle-like shape by global deformation.[25] This difference can be attributed to the adsorption of the vesicle on the interface. Continuously reducing V_w/V_0 leads to more inward bucklings over the vesicle.

Now, we examine the variation of some characteristic geometric parameters of the vesicle in the morphological transformation of the fluid vesicle. The definitions for the vesicle height H, diameter D, and contact angle θ are given in Figure 3. Simulation results for the dependence of H, D, H/D,
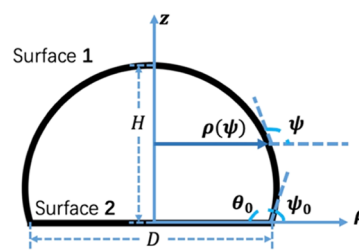
Figure 3. $\rho(\psi)$-representation of the vesicle geometry. D is the transverse extension (diameter) of the vesicle on the substrate. H is the vesicle thickness. z-Axis is the axis of rotation symmetry. θ_0 is the contact angle, $\psi_0 = \pi - \theta_0$.

and θ on the degree of dehydration V_w/V_0 are presented in Figure 4a−d. With the reduction of vesicle volume, the vesicle height decreases faster than the increase of its diameter, as shown in Figure 4a,b, respectively. Consequently, with the reduction of V_w/V_0, the ratio H/D decreases, as shown in Figure 4c. It indicates the dehydration-caused flattening of the vesicle. Figure 4d shows that the contact angle θ reduces with the progress of dehydration. Here, we emphasize that this behavior is fundamentally distinct from the case of an ordinary liquid droplet. While the equilibrium contact angle of the liquid droplet is purely determined by the hydrophilicity of the substrate, the establishment of the equilibrium contact angle of our vesicle system results from the competition of the bending energy and the surface energy of the vesicle under the constraint conditions of varying volume, which will be discussed in detail later. In comparison with the hydrophilicity-driven deformation of vesicles, the volume-driven scheme has proven to be more efficient in creating richer morphologies due to the relaxation of the constraint of fixed volume.[22−26,29]

In the following, we perform analytical analysis to explore the mechanism underlying the shape transformation of the fluid vesicles. In our model, the total free energy consists of two parts: the elastic bending energy and the surface energy. In the deformation of the vesicle sitting on the substrate, the variation of the shape and the contact area of the vesicle with the substrate leads to the change of the bending energy and the surface energy, respectively. We employ the Helfrich model to
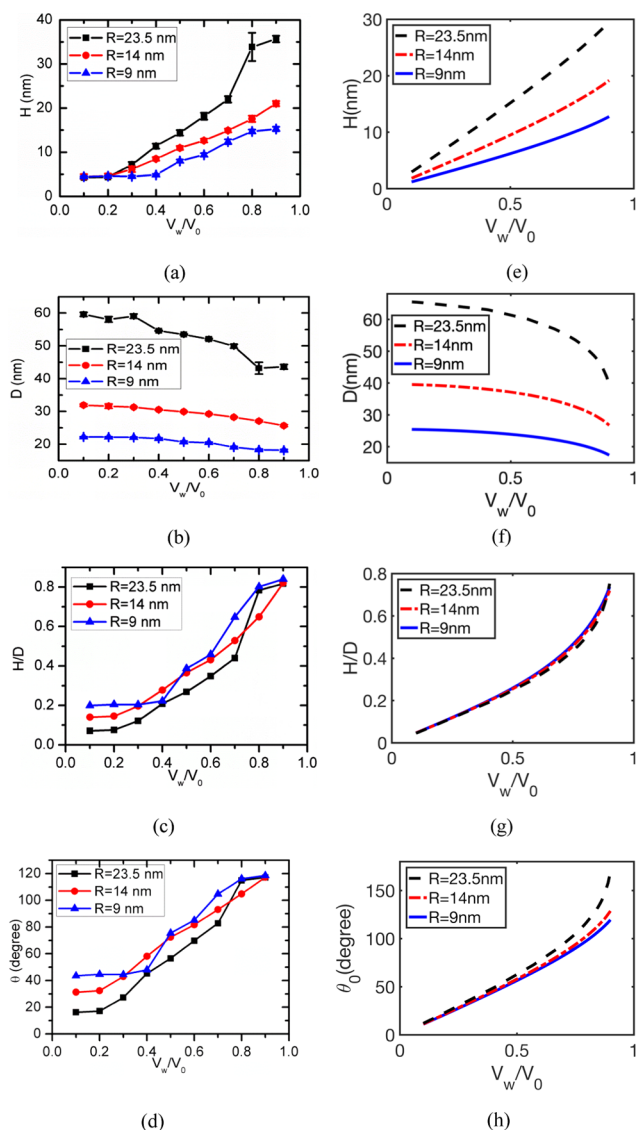
Figure 4. Dependence of the characteristic geometric parameters of the vesicle on its volume V_w from simulations and solutions of the Euler−Lagrange equation. The area of the vesicle is fixed as A_0. $R = \sqrt{A_0/4\pi}$. The largest volume of a vesicle of area A_0 is $V_0 = 4\pi R^3/ 3 = A_0^{3/2}/6\sqrt{\pi}$, which is the maximum allowed volume of a vesicle with the given surface area. H (a, e), D (b, f), H/D (c, g), and θ_0 (d, h) are the thickness, diameter, their ratio, and the contact angle, respectively [see (Figure 3)]. The simulation results are on the left (a−d). Results of solutions of the Euler−Lagrange equation are on the right (e−h). $l_c = 15$ nm.

compute the bending energy.[48] The total free energy of the vesicle is

$$F = \int_1 \sigma_1 \, dA + \int_1 \kappa_b (2H)^2 \, dA + \int_2 \sigma_2 \, dA \qquad (1)$$

where the first two terms are the surface energy and the bending energy of the upper part of the vesicle in contact with the solution (denoted surface 1) and the last term is that of the lower part of the vesicle in contact with the substrate (denoted surface 2). σ_1 and σ_2 are the surface tension of the associated surfaces, κ_b is the bending rigidity, and H is the mean curvature. Due to the affinity between the vesicle and the substrate, σ_2 is smaller than σ_1. The equilibrium shape of the

vesicle results from the competition of the bending energy and the surface energy, and it is a minimum of the total free energy.

In our calculations, we model the vesicle as an axisymmetric geometric object to capture the characteristic geometric parameters like the thickness and the transverse extension (characterized by diameter D as defined in Figure 3) of the vesicle as well as the contact angle. We employ the $\rho(\psi)$ representation to characterize the vesicle shape,[49] as shown in the schematic plot in Figure 3. ρ is the horizontal distance from a point on the surface to the axis of rotation symmetry, which is chosen as the z-axis. ψ is the angle between the tangent vector on the vesicle profile and the ρ-axis. It is straightforward to obtain the following geometric relations

$$dz = \rho' \tan\psi \, d\psi$$

$$2H = \frac{\cos\psi}{\rho'} + \frac{\sin\psi}{\rho}$$

$$dA = \frac{2\pi\rho\rho'}{\cos\psi} d\psi$$

$$dV = \pi\rho^2\rho' \tan\psi \, d\psi$$

and derive the expression of the total free energy

$$F = \sigma_1 \int_{\psi_0}^{\pi} \frac{2\pi\rho\rho'}{\cos\psi} d\psi + \kappa_b \int_{\psi_0}^{\pi} \left(\frac{\cos\psi}{\rho'} + \frac{\sin\psi}{\rho} \right)^2 \frac{2\pi\rho\rho'}{\cos\psi} d\psi$$
$$+ \sigma_2 \pi \rho_0^2 \qquad (2)$$

Now, we search for the equilibrium shape of the vesicle with the given surface area and volume. To solve this constrained variational problem, we adopt the strategy of first solving the unconstrained variational problem under the boundary conditions of $\psi(z = 0) = \psi_0$, $\rho(\psi_0) = \rho_0$, and $\rho(\pi) = 0$, and then picking up the solutions satisfying the constraints of the given area and volume from the abundant equilibrium shapes accessible by adjusting the boundary conditions. The Euler−Lagrange equation associated with eq 2 under the above-mentioned boundary conditions determines the equilibrium shape of the vesicle. The Euler−Lagrange equation is

$$\rho'' = -\frac{\rho' \tan\psi}{2\rho^2}[\rho'^2(1 + \sec^2\psi + l_c^{-2}\rho^2 \sec^2\psi) + \rho^2$$
$$- 2\rho\rho' \cot\psi] \qquad (3)$$

Here, the characteristic length l_c, which is defined as $l_c = \sqrt{\kappa/(\sigma_1 - \sigma_2)}$, is to show that the vesicle shape is determined by the competition of the bending energy and the difference of the surface energy. In the limit of large l_c, the equilibrium shape of the vesicle is dominated by the bending energy. By ignoring the term including l_c at the right-hand side of eq 3, we obtain the solution: $(\psi) = \rho_0 \sin\psi/\sin\psi_0$, which describes a spherical surface. In the opposite regime of small l_c, the surface energy dominates over the bending energy, and $\sigma_1 \gg \sigma_2$. In other words, in this regime, the vesicle is very flexible and the vesicle has a much larger affinity with the solution than with the substrate. Our numerical solution to eq 3 shows that the vesicle becomes flattened to avoid contact with the solution in the regime of small l_c.

We solve eq 3 numerically, and the results are presented in Figure 4e−h. These results coincide with the observations in simulations in Figure 4a−d. Specifically, the salient features in the equilibrium shapes of the vesicles revealed in simulations,

including the dehydration-driven flattening of the vesicle and the variation of the contact angle, are also derived from our model, as shown in Figure 4. Regarding the value of l_c, we specify a series of values and generate the corresponding curves of H vs V_w/V_0, D vs V_w/V_0, and H/D vs V_w/V_0. By comparing these numerically solved curves with the MD simulation results, we find that the value of l_c of the simulated vesicle system is about 15 nm. Notably, from Figure 4e,f, we see that the H- and D-curves for larger vesicles have a stronger dependence on the vesicle volume. This phenomenon is mainly due to the surface tension effect since the bending energy is weakly dependent on the vesicle size.[49,50] In contrast, the $H/D-V_w$ curve exhibits a much weaker dependence on vesicle size R.

We proceed to discuss the variation of the interaction potential energies of a draining fluid vesicle. Figure 5 is a plot
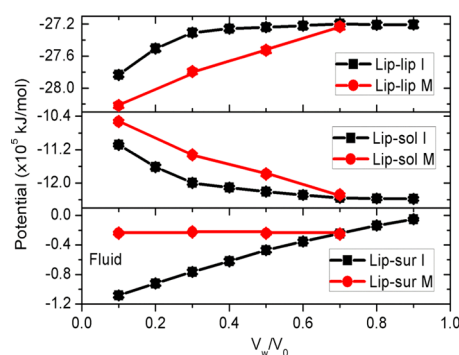
Figure 5. Lipid−lipid, lipid−solution, and lipid−surface potential energies of a fluid vesicle on a SiO$_2$ substrate as a function of V_w/V_0. V_w is the volume of the vesicle, and V_0 is the initial volume of the vesicle before dehydration occurs. The symbols I and M indicate the two dynamic protocols to remove water from the vesicle in simulations.

of the potential energies, including the Lennard-Jones and electrostatic interactions of lipid−lipid, lipid−solution, and lipid−surface. We see that the energy curve exhibits a bifurcation phenomenon for the protocols I and M, which is highly coupled with the gyration curve in Figure 2. Specifically, for the protocol I, with spreading of the vesicle on the interface, both the distances between the top and bottom bilayers and the lipid−solution contact area decrease. Therefore, the lipid−lipid interaction energy increases and the lipid−solution interaction energy decreases. For the protocol M, inward buckling shrinks the vesicle and thus leads to the increase of the lipid−lipid interaction energy. Figure 5 also shows that, in comparison with the protocol I, the lipid−surface interaction energy of the protocol M is almost invariant. This indicates that the vesicle and the interface tend to maintain an almost constant contact area in the inward-buckling featured morphological transformations. Buckling of materials is a common phenomenon in cells, elastic sheets,[51] and virus systems.[52] In general, buckling of elastic systems occurs when the reduction of the accumulated in-plane strain energy exceeds the increase of the bending energy. In contrast, in our system, buckling of the vesicles is caused by the constraint of fixed volume. With the reduction of the vesicle volume, which is realized by the removal of water inside the vesicle, the vesicle will buckle inward to reduce the volume even if the deformation is energetically costly.

Shape Transformations of Crystalline Vesicles. Now, we discuss the morphological transformation of crystalline vesicles adsorbed on the interface in the dehydration process. In comparison with fluid vesicles, largely due to the rigidity of crystalline order, free-standing crystalline vesicles tend to form diverse polyhedral shapes, as revealed by theory,[36,37] experiments,[33−35] and our previous simulation work.[25] It is of interest to inquire about the morphological transformation of a crystalline vesicle adsorbed on the liquid−solid interface. Figure 6 shows the variation of the mean-squared radius of
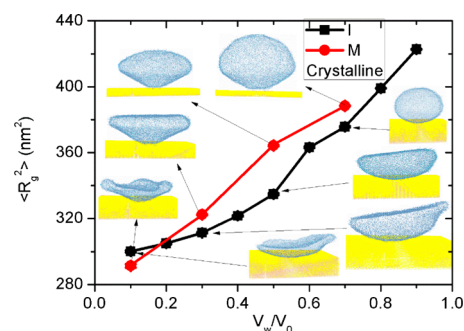
Figure 6. Plot of the mean-squared radius of gyration of a crystalline vesicle on a SiO$_2$ substrate versus V_w/V_0. V_w is the volume of the vesicle, and V_0 is the initial volume of the vesicle before dehydration occurs. Symbols I and M indicate the two dynamic protocols to remove water from the vesicle in simulations.

gyration for the crystalline vesicle in the dehydration process. We also see morphological bifurcation with the distinct protocols I and M, but not as sharp as that in the case of a fluid vesicle. Furthermore, due to the rigidity of crystalline order, a crystalline vesicle can maintain the original spherical shape for a longer duration than a fluid vesicle in the dehydration process. At $V_w/V_0 = 0.7$, the fluid vesicle becomes prolate (see Figure 2), whereas the crystalline vesicle is still spherical (see Figure 6).

Figure 6 shows that a prominent feature over a deformed crystalline vesicle is the appearance of local flat planes to reduce curvature energy cost; their size grows with the progress of dehydration. With the protocol I, the tiny flat plane initially forms on the top of the vesicle and gradually grows to occupy half of the sphere at about $V_w/V_0 = 0.5$, and the entire vesicle ultimately evolves into an inwardly buckled bowl-like shape at $V_w/V_0 = 0.1$, as shown in Figure 6. This sequence of the morphological transformation largely follows that of a free-standing vesicle, except for the final shape.[25]

For the protocol M, however, the shape of the crystalline vesicle follows a sequence that is quite different from the case of the free-standing vesicle. Continuous dehydration finally deforms the crystalline vesicle to an inwardly buckled, double-layered conelike shape, as shown in the inset at $V_w/V_0 = 0.3$ in Figure 6. Since the Gaussian curvature over the conic region is zero, the appearance of the conic shape is energetically favored according to the Helfrich model.[48] By recalling the case of free-standing crystalline vesicles, we speculate that the formation of the zero-curvature conic region is through the merging of several preexisting flat planes over the vesicle triggered by the sudden loss of interior water. This speculation is supported by the identification of flat planes over the conic region by careful examination of the three-dimensional vesicle structure. Further

reduction of V_w/V_0 leads to shape fluctuation along the edge of the cone, as shown in the inset at $V_w/V_0 = 0.1$.

In Figure 7, we show the variation of the interaction potential energies of a draining crystalline vesicle. For the
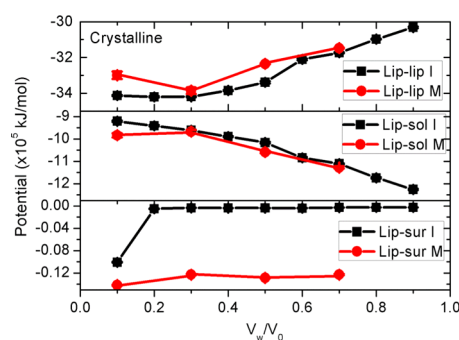
Figure 7. Lipid−lipid, lipid−solution, and lipid−surface potential energies of a crystalline vesicle on a SiO$_2$ substrate as a function of V_w/V_0. V_w is the volume of the vesicle, and V_0 is the initial volume of the vesicle before dehydration occurs. Symbols I and M indicate the two dynamic protocols to remove water from the vesicle in simulations.

protocol M, we see that the energy curves of lipid−lipid and lipid−solution interactions exhibit nonmonotonous behavior when $V_w/V_0 < 0.3$, which corresponds to the event of inward budding on the vesicle. In contrast, the corresponding energy curves for the case of the fluid vesicle are monotonously varying in the dehydration process. Furthermore, for the protocol I, we notice the appearance of a saturation plateau in the curve of the lipid−lipid interaction energy in the opposite regimes of small and large V_w/V_0 for the crystalline and fluid vesicles, respectively. For the variation of lipid−solution interaction energy presented From Figure 7, we also see that the lipid−solution interaction energy is almost invariant, except at $V_w/V_0 = 0.1$. This suggests that the contact area of the crystalline vesicle and the interface is almost invariant until the final stage of the dehydration process.

Finally, we briefly discuss the influence of adsorption strength and vesicle size on the morphology of crystalline vesicles, and the results are presented in Figure 8. Under relatively weak adsorption, the smaller vesicle exhibits a similar morphological transformation to that of the larger vesicle by comparison of the lower vesicles in Figure 8a,b. For larger vesicles, enhancing adsorption strength tends to form irregular polyhedral shapes, as shown in Figure 8b. The shape irregularity in larger vesicles may be caused by the longer response time of the system to coordinate the inward bucklings of flat planes over the vesicle.

CONCLUSIONS

In summary, we investigate the dehydration-driven morphological transformation of both fluid and crystalline vesicles adsorbed on the liquid−solid interface using the combination of molecular dynamics simulations and analytical theory. We find the bifurcation in the deformation of these two types of vesicles under slow and fast dehydration modes. Specifically, we identify inward-buckling-driven large deformations, including stomatocyte-like shapes for fluid vesicles and double-layered bowl-like and conelike shapes for crystalline vesicles. This work demonstrates the combination of surface adsorption and the dynamic dehydration protocol as an effective strategy
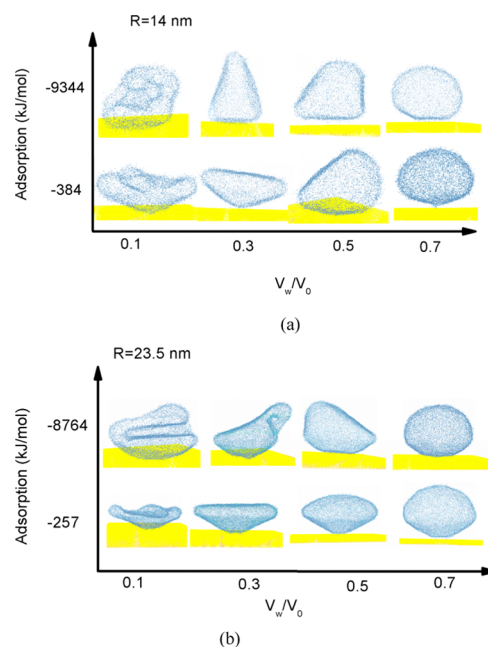
Figure 8. Shape evolution of adsorbed crystalline vesicles under protocol M at varying vesicle size and adsorption strength.

to enlarge the vesicle shape space. It has implications toward versatile control and engineering of vesicles on the interface.

AUTHOR INFORMATION

Corresponding Authors
*E-mail: jysu@iccas.ac.cn. Phone: +8613584050933.
*E-mail: zyao@sjtu.edu.cn. Phone: +8615002105374.
ORCID
Jiaye Su: 0000-0001-9894-578X
Notes
The authors declare no competing financial interest.

REFERENCES

(1) Markvoort, A. J.; van Santen, R. A.; Hilbers, P. A. J. Vesicle Shapes from Molecular Dynamics Simulations. *J. Phys. Chem. B* **2006**, *110*, 22780−22785.

(2) Liu, X.; Zhou, G.; Huo, F.; Wang, J.; Zhang, S. Unilamellar Vesicle Formation and Microscopic Structure of Ionic Liquids in Aqueous Solutions. *J. Phys. Chem. C* **2016**, *120*, 659−667.

(3) Markvoort, A. J.; Spijker, P.; Smeijers, A. F.; Pieterse, K.; van Santen, R. A.; Hilbers, P. A. J. Vesicle Deformation by Draining: Geometrical and Topological Shape Changes. *J. Phys. Chem. B* **2009**, *113*, 8731−8737.

(4) Versluis, F.; Tomatsu, I.; Kehr, S.; Fregonese, C.; Tepper, A. W. J. W.; Stuart, M. C. A.; Ravoo, B. J.; Koning, R. I.; Kros, A. Shape and Release Control of a Peptide Decorated Vesicle through pH Sensitive

Orthogonal Supramolecular Interactions. *J. Am. Chem. Soc.* **2009**, *131*, 13186−13187.

(5) van der Heide, T.; Stuart, M. C. A.; Poolman, B. On the Osmotic Signal and Osmosensing Mechanism of an ABC Ttransport System for Glycine Betaine. *EMBO J.* **2001**, *20*, 7022−7032.

(6) Liu, P.; Li, J.; Zhang, Y. W. Pressure-Temperature Phase Diagram for Shapes of Vesicles: A Coarse-Grained Molecular Dynamics Study. *Appl. Phys. Lett.* **2009**, *95*, No. 143104.

(7) Dinsmore, A. D.; Hsu, M. F.; Nikolaides, M. G.; Marquez, M.; Bausch, A. R.; Weitz, D. A. Colloidosomes: Selectively Permeable Capsules Composed of Colloidal Particles. *Science* **2002**, *298*, 1006−1009.

(8) Shojaei, H. R.; Muthukumar, M. Adsorption and Encapsulation of Flexible Polyelectrolytes in Charged Spherical Vesicles. *J. Chem. Phys.* **2017**, *146*, No. 244901.

(9) Mable, C. J.; Gibson, R. R.; Prevost, S.; McKenzie, B. E.; Mykhaylyk, O. O.; Armes, S. P. Loading of Silica Nanoparticles in Block Copolymer Vesicles during Polymerization-Induced Self-Assembly: Encapsulation Efficiency and Thermally Triggered Release. *J. Am. Chem. Soc.* **2015**, *137*, 16098−16108.

(10) Shojaei, H. R.; Muthukumar, M. Translocation of an Incompressible Vesicle through a Pore. *J. Phys. Chem. B* **2016**, *120*, 6102−6109.

(11) Rahman, M. M.; Ueda, M.; Hirose, T.; Ito, Y. Spontaneous Formation of Gating Lipid Domain in Uniform-Size Peptide Vesicles for Controlled Release. *J. Am. Chem. Soc.* **2018**, *140*, 17956−17961.

(12) He, K.; Marsland, R., III; Upadhyayula, S.; Song, E.; Dang, S.; Capraro, B. R.; Wang, W.; Skillern, W.; Gaudin, R.; Ma, M.; Kirchhausen, T. Dynamics of Phosphoinositide Conversion in Clathrin-Mediated Endocytic Traffic. *Nature* **2017**, *552*, 410−414.

(13) Mirigian, S.; Muthukumar, M. Kinetics of Particle Wrapping by a Vesicle. *J. Chem. Phys.* **2013**, *139*, No. 044908.

(14) Sherman, S. E.; Xiao, Q.; Percec, V. Mimicking Complex Biological Membranes and Their Programmable Glycan Ligands with Dendrimersomes and Glycodendrimersomes. *Chem. Rev.* **2017**, *117*, 6538−6631.

(15) Towns, E. N.; Parikh, A. N.; Land, D. P. Influence of Vesicle Size and Aqueous Solvent on Intact Phospholipid Vesicle Adsorption on Oxidized Gold Monitored Using Attenuated Total Reflectance Fourier Transform Infrared Spectroscopy. *J. Phys. Chem. C* **2015**, *119*, 2412−2418.

(16) Datta, S. S.; Kim, S. H.; Paulose, J.; Abbaspourrad, A.; Nelson, D. R.; Weitz, D. A. Delayed Buckling and Guided Folding of Inhomogeneous Capsules. *Phys. Rev. Lett.* **2012**, *109*, No. 134302.

(17) Talbot, E. L.; Kotar, J.; Parolini, L.; Michele, L. D.; Cicuta, P. Thermophoretic Migration of Vesicles Depends on Mean Temperature and Head Group Chemistry. *Nat. Commun.* **2017**, *8*, No. 15351.

(18) Kim, S.; Bellouard, C.; Eastoe, J.; Canilho, N.; Rogers, S. E.; Ihiawakrim, D.; Ersen, O.; Pasc, A. Spin State As a Probe of Vesicle Self-Assembly. *J. Am. Chem. Soc.* **2016**, *138*, 2552−2555.

(19) Yu, M.; Lira, R. B.; Riske, K. A.; Dimova, R.; Lin, H. Ellipsoidal Relaxation of Deformed Vesicles. *Phys. Rev. Lett.* **2015**, *115*, No. 128303.

(20) Farsi, Z.; Preobraschenski, J.; van den Bogaart, G.; Riedel, D.; Jahn, R.; Woehler, A. Single-Vesicle Imaging Reveals Different Transport Mechanisms between Glutamatergic and GABAergic Vesicles. *Science* **2016**, *351*, 981−984.

(21) Jung, J. H.; Szule, J. A.; Marshall, R. M.; McMahan, U. J. Variable Priming of a Docked Synaptic Vesicle. *Proc. Natl. Acad. Sci. U.S.A.* **2016**, *113*, E1098−E1107.

(22) Seifert, U. Configurations of Fluid Membranes and Vesicles. *Adv. Phys.* **1997**, *46*, 13−137.

(23) Seifert, U.; Berndl, K.; Lipowsky, R. Shape Transformations of Vesicles: Phase Diagram for Spontaneous-Curvature and Bilayer-Coupling Models. *Phys. Rev. A* **1991**, *44*, 1182−1202.

(24) Miao, L.; Seifert, U.; Wortis, M.; Döbereiner, H. G. Budding Transitions of Fluid-Bilayer Vesicles: The Effect of Area-Difference Elasticity. *Phys. Rev. E* **1994**, *49*, 5389−5407.

(25) Su, J.; Yao, Z.; de la Cruz, M. O. Vesicle Geometries Enabled by Dynamically Trapped States. *ACS Nano* **2016**, *10*, 2287−2294.

(26) Yuan, H. Y.; Huang, C. J.; Zhang, S. L. Dynamic Shape Transformations of Fluid Vesicles. *Soft Matter* **2010**, *6*, 4571−4579.

(27) Klauda, J. B. Perspective: Computational Modeling of Accurate Cellular Membranes with Molecular Resolution. *J. Chem. Phys.* **2018**, *149*, No. 220901.

(28) Marrink, S. J.; Corradi, V.; Souza, P. C. T.; Ingolfsson, H. I.; Tieleman, D. P.; Sansom, M. S. P. Computational Modeling of Realistic Cell Membranes. *Chem. Rev.* **2019**, DOI: 10.1021/acs.chemrev.8b00460.

(29) Li, X. Shape Transformations of Bilayer Vesicles from Amphiphilic Block Copolymers: A Dissipative Particle Dynamics Simulation Study. *Soft Matter* **2013**, *9*, 11663−11670.

(30) Dimitrievski, K.; Kasemo, B. Influence of Lipid Vesicle Composition and Surface Charge Density on Vesicle Adsorption Events: A Kinetic Phase Diagram. *Langmuir* **2009**, *25*, 8865−8869.

(31) Abraham, S.; Heckenthaler, T.; Bandyopadhyay, D.; Morgenstern, Y.; Kaufman, Y. Quantitative Description of the Vesicle Fusion Mechanism on Solid Surfaces and the Role of Cholesterol. *J. Phys. Chem. C* **2018**, *122*, 22985−22995.

(32) Dimitrievski, K.; Kasemo, B. Simulations of Lipid Vesicle Adsorption for Different Lipid Mixtures. *Langmuir* **2008**, *24*, 4077−4091.

(33) Leung, C. Y.; Palmer, L. C.; Qiao, B.; Kewalramani, S.; Sknepnek, R.; Newcomb, C. J.; Greenfield, M. A.; Vernizzi, G.; Stupp, S. I.; Bedzyk, M. J.; de la Cruz, M. O. Molecular Crystallization Controlled by pH Regulates Mesoscopic Membrane Morphology. *ACS Nano* **2012**, *6*, 10901−10909.

(34) Leung, C. Y.; Palmer, L. C.; Kewalramani, S.; Qiao, B.; Stupp, S. I.; de la Cruz, M. O.; Bedzyk, M. J. Crystalline Polymorphism Induced by Charge Regulation in Ionic Membranes. *Proc. Natl. Acad. Sci. U.S.A.* **2013**, *110*, 16309−16314.

(35) Greenfield, M. A.; Palmer, L. C.; Vernizzi, G.; de la Cruz, M. O.; Stupp, S. I. Buckled Membranes in Mixed-Valence Ionic Amphiphile Vesicles. *J. Am. Chem. Soc.* **2009**, *131*, 12030−12031.

(36) Yong, E. H.; Nelson, D. R.; Mahadevan, L. Elastic Platonic Shells. *Phys. Rev. Lett.* **2013**, *111*, No. 177801.

(37) Vernizzi, G.; Sknepnek, R.; de la Cruz, M. O. Platonic and Archimedean Geometries in Multicomponent Elastic Membranes. *Proc. Natl. Acad. Sci. U.S.A.* **2011**, *108*, 4292−4296.

(38) Cebecauer, M.; Amaro, M.; Jurkiewicz, P.; Sarmento, M. J.; Šachl, R.; Cwiklik, L.; Hof, M. Membrane Lipid Nanodomains. *Chem. Rev.* **2018**, *118*, 11259−11297.

(39) Qiao, B.; de la Cruz, M. O. Driving Force for Water Permeation Across Lipid Membranes. *J. Phys. Chem. Lett.* **2013**, *4*, 3233−3237.

(40) Su, J.; Zhao, Y.; Fang, C.; Shi, Y. Asymmetric Osmotic Water Permeation through a Vesicle Membrane. *J. Chem. Phys.* **2017**, *146*, No. 204902.

(41) Ortony, J. H.; Qiao, B.; Newcomb, C. J.; Keller, T. J.; Palmer, L. C.; Deiss-Yehiely, E.; de la Cruz, M. O.; Han, S.; Stupp, S. I. Water Dynamics from the Surface to the Interior of a Supramolecular Nanostructure. *J. Am. Chem. Soc.* **2017**, *139*, 8915−8921.

(42) Yanagisawa, M.; Imai, M.; Taniguchi, T. Shape Deformation of Ternary Vesicles Coupled with Phase Separation. *Phys. Rev. Lett.* **2008**, *100*, No. 148102.

(43) Hess, B.; Kutzner, C.; van der Spoel, D.; Lindahl, E. GROMACS 4: Algorithms for Highly Efficient, Load-Balanced, and Scalable Molecular Simulation. *J. Chem. Theory Comput.* **2008**, *4*, 435−447.

(44) Monticelli, L.; Kandasamy, S. K.; Periole, X.; Larson, R. G.; Tieleman, D. P.; Marrink, S. J. The MARTINI Coarse Grained Force Field: Extension to Proteins. *J. Chem. Theory Comput.* **2008**, *4*, 819−834.

(45) Marrink, S. J.; de Vries, A. H.; Mark, A. E. Coarse Grained Model for Semiquantitative Lipid Simulations. *J. Phys. Chem. B* **2004**, *108*, 750−760.

(46) Marrink, S. J.; Tieleman, D. P. Perspective on the Martini Model. *Chem. Soc. Rev.* **2013**, *42*, 6801−6822.

(47) Berendsen, H. J. C.; Postma, J. P. M.; van Gunsteren, W. F.; DiNola, A.; Haak, J. R. Molecular Dynamics with Coupling to an External Bath. *J. Chem. Phys.* **1984**, *81*, 3684−3690.

(48) Helfrich, W. Elastic Properties of Lipid Bilayers: Theory and Possible Experiments. *Z. Naturforsch., C* **1973**, *28*, 693−703.

(49) Ou-Yang, Z. C.; Liu, J.; Xie, Y. *Geometric Methods in the Elastic Theory of Membranes in Liquid Crystal Phases*; World Scientific, 1999.

(50) Yao, Z.; Sknepnek, R.; Thomas, C. K.; de la Cruz, M. O. Shapes of Pored Membranes. *Soft Matter* **2012**, *8*, 11613−11619.

(51) Audoly, B.; Pomeau, Y. *Elasticity and Geometry*; World Scientific, 2000.

(52) Lidmar, J.; Mirny, L.; Nelson, D. R. Virus Shapes and Buckling Transitions in Spherical Shells. *Phys. Rev. E* **2003**, *68*, No. 051910.